

Natural neighbour Petrov-Galerkin Method for Shape Design Sensitivity Analysis

Kai Wang¹, Shenjie Zhou^{1,2}, Zhifeng Nie¹ and Shengli Kong¹

Abstract: The natural neighbour Petrov-Galerkin method (NNPG) is one of the special cases of the generalized meshless local Petrov-Galerkin method (MLPG). This paper demonstrates the NNPG can be successfully used in design sensitivity analysis in 2D elasticity. The design sensitivity analysis method based on the local weak form (DSA-LWF) in the NNPG context is proposed. In the DSA-LWF, the local weak form of governing equation is directly differentiated with respect to design variables and discretized with NNPG to obtain the sensitivities of structural responds. The calculation of derivatives of shape functions with respect to design variables is avoided. No background meshes are needed to integrate the weak form, no assembly process is needed to generate the global stiffness matrix and no user-defined parameters are used as well. Three numerical examples are solved using DSA-LWF and the results show the proposed method gives very accurate solutions for these problems.

Keyword: shape design sensitivity analysis; meshless method; Petrov-Galerkin method; natural neighbour interpolation

1 Introduction

Gradient-based methods are widely used in shape optimization problems. In these methods, the shape design sensitivity analysis (DSA) is concerned with finding the variation of structural responses (displacement, stresses, etc.) with respect to design variables, which describe the geometry of the domain [Lacroix and Bouillard (2003)].

These sensitivities are needed in order to provide the gradients of the objective function or constraints. An accurate computation of sensitivity information plays a critical role in the shape optimization and can reduce the computational costs [Kim, Choi and Botkin (2003)].

There are several methods which can be employed in design sensitivity analysis. Generally, there are four different types, namely finite difference, discrete, continuum, and computational derivatives. Among these methods, the continuum-based DSA method is widely used in design sensitivity analysis and shape optimization problems [Lacroix and Bouillard (2003); Kim, Choi and Botkin (2003); Bobaru and Mukherjee (2001); Bobaru and Mukherjee (2002); Grindeanu, Kim, Choi and Chen (2002); Kim, Yi and Choi (2002); Chang, Choi, Tsai, Chen, Choi and Yu (1995)]. In this kind of method, the continuous deformation of the structure is simulated and the material derivative concept is used to define the sensitivities of structural responds.

The finite element methods (FEMs) have become the most popular numerical approach in various engineering applications. However, the FEMs are not convenient for shape optimization problems due to the use of mesh. Firstly, the remeshing process is often inevitable in optimization iterations when the mesh gets distorted too much. Secondly, it is necessary to modify the geometry and to generate a new mesh in order to compute the sensitivities. Unfortunately, for most of the existing methods, a restriction is that the perturbed mesh must have the same topology as the initial one. This can not be satisfied if the mesh is generated with the aim of controlling its accuracy [Lacroix and Bouillard (2003)].

Meshless methods [Belytschko, Krongauz, Or-

¹ School of Mechanical Engineering, Shandong University, No.73 Jingshi Road, Jinan, 250061, P. R. China

² Corresponding author. Email: zhousj@sdu.edu.cn

gan, Fleming and Krysl (1996); Atluri and Zhu (1998); Cueto, Sukumar, Calvo, Cegoñino and Doblaré (2003); Liu, Jun, Zhang (1995)] as alternative methods to FEMs have attracted much attention these years. As the approximation of solution variables is constructed by scattered nodes instead of elements, meshless methods are more suitable for moving boundary problems, large deformation problems, high speed impact problems, etc. With regard to the DSA computation and shape optimization, because no mesh is needed to interpolate either field variables or their sensitivities, the aforementioned inconveniences of use of FEM are resolved. Many researchers take the advantages of meshless methods in DSA computations [Lacroix and Bouillard (2003); Kim, Choi and Botkin (2003); Bobaru and Mukherjee (2001); Bobaru and Mukherjee (2002); Grindeanu, Kim, Choi and Chen (2002)]. Lacroix and Bouillard (2003) proposed a DSA approach by coupling the element free Galerkin method (EFG) [Belytschko, Lu and Gu (1994)] with the FEM. Bobaru and Mukherjee (2001, 2002) developed a continuum-based DSA method in the EFG context and used in shape optimization problems of both linear elastic and thermo elastic solids. In their method, the derivative of global Galerkin weak form of equilibrium equation with respect to each design variable is computed by direct differentiation method (DDM) [Kim, Choi and Botkin (2003); Bobaru and Mukherjee (2001); Bobaru and Mukherjee (2002); Grindeanu, Kim, Choi and Chen (2002)]. Numerical methods for continuum-based shape design sensitivity analysis and optimization using reproducing kernel particle method (RKPM) [Liu, Jun and Zhang (1995)] were proposed by Grindeanu, Kim, Choi and Chen (2002) and Kim, Yi and Choi (2002).

Many meshless methods have been developed so far. Among these methods, the meshless local Petrov-Galerkin method (MLPG) originally proposed by Atluri and Zhu (1998) is one of the most prominent methods, because it is not only a truly meshless method but also a generalized framework that could be used to derive other meshless methods [Atluri, Kim and Cho (1999); Atluri

and Shen (2002)]. Many researchers are optimistic about this method and use it in their research fields. In recent years, the MLPG has made great progress in many aspects. Several new methods are proposed within the framework of MLPG [Atluri and Shen (2002); Atluri, Liu and Han (2006a); Atluri, Liu and Han (2006b); Atluri, Han and Rajendran (2004); Vavourakis, Sellountos and Polyzos (2006); Vavourakis and Polyzos (2007)]. A wide variety of engineering problems are solved by the MLPG type meshless methods [Han and Atluri (2004); Shen and Atluri (2004); Andreaus, Batra and Porfiri (2005); Han, Rajendran and Atluri (2005); Han, Liu, Rajendran et al. (2006); Ching and Chen (2006); Gao, Liu and Liu (2006); Sladek, Sladek and Zhang et al. (2007); Jarak, Soric and Hoster (2007)].

The natural neighbour Petrov-Galerkin method (NNPG) [Wang, Zhou and Shan (2005)] is one of the special cases of the generalized MLPG. As this method is quite efficient and easy to implement, it is suitable for DSA computation and shape optimization where high efficiency is desired. This paper demonstrates the NNPG can be successfully used for DSA computation and shape optimization in 2D elasticity. The design sensitivity analysis method based on the local weak form (DSA-LWF) in the NNPG context is proposed. The material derivative concept is adopted in the DSA-LWF, and the continuous formulation of design sensitivity analysis is derived by directly differentiating the local weak form of equilibrium equations. The discretization of the continuous formulation and the numerical implementation are also proposed. Three numerical examples are presented to test the validity and accuracy of the DSA-LWF method.

This paper is organized as follows: In section 2, the natural neighbour Petrov-Galerkin method is briefly reviewed. In section 3, the DSA-LWF method under the NNPG framework is proposed in details. In section 4, three numerical examples are presented to test the proposed method. This paper ends with the conclusions in section 5.

2 Review of natural neighbour Petrov-Galerkin method

Under the framework of MLPG, new meshless method can be derived if the trial function, test function and integration method are carefully chosen [Atluri, Kim and Cho (1999); Atluri and Shen (2002)]. The natural neighbour Petrov-Galerkin method (NNPG) [Wang, Zhou and Shan (2005)] can be considered as a special case of MLPG. This method is developed to alleviate the task of imposition of essential boundary condition in classical MLPG. In the NNPG, the non-Sibsonian interpolation is used to approximate the trial function, and linear FEM shape function is chosen to be the test function. The Delaunay tessellation is used to construct the nodal local sub-domain Ω_s , which is coincident with the support of nodal test function.

In each nodal local sub-domain Ω_s , the local Petrov-Galerkin method [Atluri and Zhu (1998)] is used in stead of global Galerkin one. As non-Sibsonian interpolation is used to approximate the field variables, neither penalty parameters [Atluri and Zhu (1998)] nor Lagrange multipliers [Belytschko, Lu and Gu (1994)] are needed to impose the essential boundary condition. The NNPG continuous local weak form of governing equation in elasto-statics is defined as:

$$\int_{\Omega_s} \sigma_{ij} N_{Ii,j} d\Omega - \int_{L_u} N_{Ii} \sigma_{ij} n_j d\Gamma = \int_{\Omega_s} N_{Ii} b_i d\Omega + \int_{L_t} N_{Ii} \bar{t}_i d\Gamma \quad (1)$$

where $\partial\Omega_s = L_u + L_t + L_s$ is the boundary of local sub-domain, σ_{ij} is the stress tensor related to the displacement field u_i , b_i is the vector of body force, n_j is the unit outward normal vector to the boundary L_u , \bar{t}_i is the prescribed tractions on the traction boundary L_t and N_{Ii} is the test function corresponding to the nodal sub-domain Ω_s . To obtain the discrete algebraic equation, the displacement of point \mathbf{x} is approximated by:

$$u^h(\mathbf{x}) = \sum_{I=1}^n \phi_I(\mathbf{x}) u_I \quad (2)$$

with

$$\phi_I(\mathbf{x}) = \frac{s_I(\mathbf{x})/h_I(\mathbf{x})}{\sum_{J=1}^n [s_J(\mathbf{x})/h_J(\mathbf{x})]} \quad (3)$$

where n is the number of natural neighbours of the point \mathbf{x} , u_I ($I=1, 2, \dots, n$) are the vectors of nodal displacements at n natural neighbours, and $\phi_I(\mathbf{x})$ is the non-Sibsonian interpolation shape function, s_I is the Lebesgue measure of the Voronoi boundary associated with node I (here is the length of Voronoi edge in 2D case), and the h_I is the distance between the evaluated point \mathbf{x} and the node I .

The discrete form can be obtained by substituting equation (2) into it equation (1):

$$\sum_{J=1}^N \mathbf{K}_{IJ} \mathbf{u}_J = \mathbf{F}_I, \quad I = 1, 2, \dots, N \quad (4)$$

where \mathbf{K}_{IJ} and \mathbf{F}_I are local stiffness matrix and force matrix corresponding to the nodal sub-domain Ω_s^I , N is the total number of the nodes in the global domain and on its boundary, \mathbf{u}_J is the matrix of nodal displacements.

As a special case of the generalized MLPG, the NNPG inherits the virtues of the MLPG [Atluri, Kim and Cho (1999)], e.g., no assembly process is needed to form the global stiffness matrix and no additional background cells are needed to integrate the weak form. Compare with the classical MLPG, the NNPG has two additional properties [Wang, Zhou and Shan (2005)]. Firstly, the calculation of non-Sibsonian interpolation shape function is more efficient than that of MLS, and the shape function has Kronecker Delta function property. This may contribute to its high efficiency. Secondly, by virtue of the test function used, the supports of integrands align with the integration domains. This may improve the accuracy of numerical integration [Dolbow and Belytschko (1999)]. All these properties, no matter inherited or intrinsic, render the NNPG a promising method for DSA computation and shape optimization.

3 Local continuum-based DSA formulation

The sensitivity of a structural response (displacement, stress) with respect to a design variable is a

kind of material derivative [Bobaru and Mukherjee (2001), Kim, Yi and Choi (2002)] which takes into account the shape variation of the structural domain due to the design variable perturbation. Let us consider the displacement vector \mathbf{u} which can be expressed as a function of the design variable $\boldsymbol{\tau}$ and of the position $\boldsymbol{\xi}$. The sensitivity of \mathbf{u} with respect to $\boldsymbol{\tau}$ is defined as [Bobaru and Mukherjee (2001)]:

$$\dot{\mathbf{u}} = \lim_{\boldsymbol{\tau} \rightarrow 0} \frac{\mathbf{u}[\boldsymbol{\xi}(\mathbf{x}, \boldsymbol{\tau}), \boldsymbol{\tau}] - \mathbf{u}(\mathbf{x}, 0)}{\boldsymbol{\tau}} = \mathbf{u}' + \nabla \mathbf{u} \cdot \mathbf{v} \quad (5)$$

In above equation, $\mathbf{v}(\mathbf{x})$ is the design velocity field [Ródenas, Fuenmayor and Tarancón, J. E. (2004)], which defines the variation of the position of each material point due to the variation of the design variable. By importing strain-displacement relation and constitutive equation [Timoshenko and Goodier (1970)], all other sensitivities (e.g., stress sensitivities $\dot{\boldsymbol{\sigma}}$) can be derived from the displacement sensitivity $\dot{\mathbf{u}}$.

3.1 Continuous DSA formulation based on NNPG local weak form

There are several methods can be used to calculate the displacement sensitivity. Among these methods, the direct differentiation method (DDM) is quite simple and widely used in shape optimization problems [Kim, Choi and Botkin (2003); Bobaru and Mukherjee (2001); Bobaru and Mukherjee (2002); Grindeanu, Kim, Choi and Chen (2002)]. Consider a structural system in the final equilibrium configuration, corresponding to a given design variable $\boldsymbol{\tau}$. The equilibrium equation for the structural system can be written as:

$$\mathbf{A}(\boldsymbol{\tau})\mathbf{u}(\boldsymbol{\tau}) = \mathbf{f}(\boldsymbol{\tau}) \quad (6)$$

The displacement field \mathbf{u} can be solved from above equation. By using DDM, the displacement sensitivity $\dot{\mathbf{u}}$ is obtained by directly differentiating equation (6) with respect to every design variables:

$$\mathbf{A}(\boldsymbol{\tau})\dot{\mathbf{u}} = \frac{d\mathbf{f}(\boldsymbol{\tau})}{d\boldsymbol{\tau}} - \frac{d\mathbf{A}(\boldsymbol{\tau})}{d\boldsymbol{\tau}}\mathbf{u}(\boldsymbol{\tau}) \quad (7)$$

As global Galerkin method dominates in numerical methods, almost all the continuum-based DSA

formulations are derived from it. In this case, the equation (6) is a global symmetric weak form of equilibrium equation. After using DDM, the equation (7) includes integrals over global domain. These integrals have to be evaluated with the aid of background meshes [Belytschko, Krongauz, Organ, Fleming and Krysl (1996)]. It is reported that the support of the integrand needs to be aligned with the background mesh to improve the accuracy of Gaussian quadrature [Dolbow and Belytschko (1999)]. However, to construct background meshes aligning with the supports of integrands is not easy for most meshless methods. Therefore, integration error is often introduced. In addition, the ‘‘assembly’’ process is always necessary to generate the stiffness matrix in these methods [Atluri and Zhu (1998)].

Under the framework of NNPG, the local weak form is used instead of global Galerkin one and a more explicit form of equation (7) is obtained by directly differentiating the continuous local weak form of governing equation (1). For example, the material derivative of first term in the left hand of the equation (1) is calculated:

$$\begin{aligned} & \int_{\Omega_s} [(\overline{\dot{\sigma}_{ij}(u)N_{i,j}}) + (\sigma_{ij}(u)N_{i,j})(v_{i,i})]d\Omega = \\ & \int_{\Omega_s} [\dot{\sigma}_{ij}(u)N_{i,j} + \sigma_{ij}(u)\overline{\dot{N}_{i,j}} + \sigma_{ij}(u)N_{i,j}(v_{i,i})]d\Omega \end{aligned} \quad (8)$$

where $\overline{\dot{N}_{i,j}} = \dot{N}_{i,j} - N_{i,k}v_{k,j}$ is the material derivative of the spatial derivative of the test function. $\dot{\sigma}_{ij}$ is the stress sensitivity, which can be obtained by importing strain-displacement relation and constitutive law:

$$\dot{\sigma}_{ij}(u) = \sigma_{i,j}(\dot{u}) - \frac{1}{2}D_{ijkl}(v_{k,j}u_{i,k} + v_{k,i}u_{j,k}) \quad (9)$$

where D_{ijkl} is the material constant tensor. Substituting equation (9) into equation (8), the material derivative of first term in the left hand of the equa-

tion (1) can be written as:

$$\begin{aligned}
& \int_{\Omega_s} \left[\overline{(\sigma_{ij}(\dot{u})N_{Ii,j})} + (\sigma_{ij}N_{Ii,j})(v_{i,i}) \right] d\Omega \\
&= \int_{\Omega_s} \sigma_{ij}(\dot{u})N_{Ii,j}d\Omega \\
&- \frac{1}{2} \int_{\Omega_s} D_{ijkl} (v_{k,j}u_{i,k} + v_{k,i}u_{j,k}) N_{Ii,j}d\Omega \\
&+ \int_{\Omega_s} \sigma_{ij}(u)(\dot{N}_{Ii,j} - N_{Ii,k}v_{k,j})d\Omega \\
&\quad + \int_{\Omega_s} \sigma_{ij}(u)N_{Ii,j}(v_{i,i})d\Omega \quad (10)
\end{aligned}$$

With similar procedures, the material derivative of equation (1) can be written as:

$$\begin{aligned}
& \int_{\Omega_s} \sigma_{ij}(\dot{u})N_{Ii,j}d\Omega \\
&- \frac{1}{2} \int_{\Omega_s} D_{ijkl} [v_{k,j}u_{i,k} + v_{k,i}u_{j,k}] N_{Ii,j}d\Omega \\
&- \int_{\Omega_s} \sigma_{ij}(u)N_{Ii,k}v_{k,j}d\Omega \\
&+ \int_{\Omega_s} \sigma_{ij}(u)(v_{i,i})N_{Ii,j}d\Omega \\
&- n_j \int_{L_u} \sigma_{ij}(\dot{u})N_{Ii}d\Gamma \\
&+ \frac{n_j}{2} \int_{L_u} D_{ijkl} [v_{k,j}u_{i,k} + v_{k,i}u_{j,k}] N_{Ii}d\Gamma \\
&- \int_{L_u} \sigma_{ij}(u)n_jN_{Ii}(v_i n_i)Hd\Gamma = \\
& \int_{\Omega_s} [\dot{b}_i + b_i(v_{i,i})]N_{Ii}d\Omega + \int_{L_t} [\dot{\bar{t}}_i + \bar{t}_i(v_i n_i)H]N_{Ii}d\Gamma
\end{aligned} \quad (11)$$

where $H = -n_{i,i}$ is the surface divergence [Borbaru and Mukherjee (2001)]. In above equation, considering strain-displacement relation and constitutive law of elasto-statics, the local continuous

DSA formulation is obtained:

$$\begin{aligned}
& \int_{\Omega_s} D_{ijkl} \frac{1}{2} (\dot{u}_{k,l} + \dot{u}_{l,k}) N_{Ii,j} d\Omega \\
&- \frac{1}{2} \int_{\Omega_s} D_{ijkl} [v_{k,j}u_{i,k} + v_{k,i}u_{j,k}] N_{Ii,j} d\Omega \\
&- \int_{\Omega_s} D_{ijkl} \frac{1}{2} (u_{k,l} + u_{l,k}) N_{Ii,k} v_{k,j} d\Omega \\
&+ \int_{\Omega_s} D_{ijkl} \frac{1}{2} (u_{k,l} + u_{l,k}) (v_{i,i}) N_{Ii,j} d\Omega \\
&- n_j \int_{L_u} D_{ijkl} \frac{1}{2} (\dot{u}_{k,l} + \dot{u}_{l,k}) N_{Ii} d\Gamma \\
&+ \frac{n_j}{2} \int_{L_u} D_{ijkl} [v_{k,j}u_{i,k} + v_{k,i}u_{j,k}] N_{Ii} d\Gamma \\
&- \int_{L_u} D_{ijkl} \frac{1}{2} (u_{k,l} + u_{l,k}) n_j N_{Ii} (v_i n_i) H d\Gamma = \\
& \int_{\Omega_s} [\dot{b}_i + b_i(v_{i,i})] N_{Ii} d\Omega + \int_{L_t} [\dot{\bar{t}}_i + \bar{t}_i(v_i n_i)H] N_{Ii} d\Gamma
\end{aligned} \quad (12)$$

3.2 NNPG discretization and numerical implementation

To avoid the derivatives of shape functions with respect to design variables, the displacement sensitivities are also approximated with non-Sibsonian interpolation:

$$\dot{u}^h(\mathbf{x}) = \sum_{l=1}^n \phi_l(\mathbf{x}) \dot{u}_l \quad (13)$$

where ϕ_l is the non-Sibsonian interpolation shape function of natural neighbour l and \dot{u}_l are the vectors of fictitious nodal displacement sensitivity. Substituting equation (2) and (13) into equation (12), the discrete form of sensitivity formulation

is obtained:

$$\begin{aligned}
& \int_{\Omega_s} D_{ijkl} \frac{1}{2} \left(\sum_{l=1}^n \phi_{l,l}(\mathbf{x}) \dot{u}_{lk} + \sum_{l=1}^n \phi_{l,k}(\mathbf{x}) \dot{u}_{ll} \right) \\
& \quad N_{li,j} d\Omega \\
& - \frac{1}{2} \int_{\Omega_s} D_{ijkl} \left[v_{k,j} \left(\sum_{l=1}^n \phi_{l,k}(\mathbf{x}) u_{li} \right) \right. \\
& \quad \left. + v_{k,i} \left(\sum_{l=1}^n \phi_{l,k}(\mathbf{x}) u_{lj} \right) \right] N_{li,j} d\Omega \\
& - \int_{\Omega_s} D_{ijkl} \frac{1}{2} \left(\sum_{l=1}^n \phi_{l,l}(\mathbf{x}) u_{lk} + \sum_{l=1}^n \phi_{l,k}(\mathbf{x}) u_{ll} \right) \\
& \quad N_{li,k} v_{k,j} d\Omega \\
& + \int_{\Omega_s} D_{ijkl} \frac{1}{2} \left(\sum_{l=1}^n \phi_{l,l}(\mathbf{x}) u_{lk} + \sum_{l=1}^n \phi_{l,k}(\mathbf{x}) u_{ll} \right) (v_{i,i}) \\
& \quad N_{li,j} d\Omega \\
& - n_j \int_{L_u} D_{ijkl} \frac{1}{2} \left(\sum_{l=1}^n \phi_{l,l}(\mathbf{x}) \dot{u}_{lk} + \sum_{l=1}^n \phi_{l,k}(\mathbf{x}) \dot{u}_{ll} \right) \\
& \quad N_{li} d\Gamma \\
& + \frac{n_j}{2} \int_{L_u} D_{ijkl} \left[v_{k,j} \left(\sum_{l=1}^n \phi_{l,k}(\mathbf{x}) u_{li} \right) \right. \\
& \quad \left. + v_{k,i} \left(\sum_{l=1}^n \phi_{l,k}(\mathbf{x}) u_{lj} \right) \right] N_{li} d\Gamma \\
& - \int_{L_u} D_{ijkl} \frac{1}{2} \left(\sum_{l=1}^n \phi_{l,l}(\mathbf{x}) u_{lk} + \sum_{l=1}^n \phi_{l,k}(\mathbf{x}) u_{ll} \right) \\
& \quad n_j N_{li} (v_i n_i) H d\Gamma \\
& = \int_{\Omega_s} [b_i + b_i(v_{i,i})] N_{li} d\Omega \\
& \quad + \int_{L_t} [\bar{t}_i + \bar{t}_i(v_i n_i) H] N_{li} d\Gamma \quad (14)
\end{aligned}$$

For simplicity, the matrix form of above equations can be written as:

$$\begin{aligned}
\sum_{J=1}^N \mathbf{K}_{IJ} \dot{\mathbf{u}}_J &= \sum_{J=1}^N (\mathbf{L}_{IJ} + \mathbf{M}_{IJ}) \mathbf{u}_J + \mathbf{Q}_I, \\
I &= 1, 2, \dots, N \quad (15)
\end{aligned}$$

where N is the total number of the nodes in the global domain and on its boundary, $\dot{\mathbf{u}}_J$ is the matrix of nodal displacements, matrices \mathbf{K}_{IJ} , \mathbf{L}_{IJ} , \mathbf{M}_{IJ} and \mathbf{Q}_I are given by

$$\mathbf{K}_{IJ} = \int_{\Omega_s} \mathbf{V}_{dI}^T \mathbf{D} \mathbf{B}_J d\Omega - \int_{L_u} \mathbf{V}_I \mathbf{N} \mathbf{D} \mathbf{B}_J d\Gamma \quad (16)$$

$$\begin{aligned}
\mathbf{L}_{IJ} &= \int_{\Omega_s} \mathbf{V}_{dI}^T \mathbf{D} \bar{\mathbf{B}}_J d\Omega + \int_{\Omega_s} \bar{\mathbf{V}}_{dI}^T \mathbf{D} \mathbf{B}_J d\Omega \\
& \quad - \int_{\Omega_s} \mathbf{V}_{dI}^T \mathbf{D} \mathbf{B}_J \operatorname{div} \mathbf{v} d\Omega \quad (17)
\end{aligned}$$

$$\mathbf{M}_{IJ} = \int_{L_u} \mathbf{V}_I \bar{\mathbf{N}} \mathbf{D} \mathbf{B}_J (\mathbf{v} \cdot \mathbf{n}) H d\Gamma - \int_{L_u} \mathbf{V}_I \bar{\mathbf{N}} \mathbf{D} \bar{\mathbf{B}}_J d\Gamma \quad (18)$$

$$\begin{aligned}
\mathbf{Q}_I &= \int_{\Omega_s} \mathbf{V}_I (\mathbf{b} + \mathbf{b} \operatorname{div} \mathbf{v}) d\Omega \\
& \quad + \int_{L_t} \mathbf{V}_I [\bar{\mathbf{t}} + \bar{\mathbf{t}}(\mathbf{v} \cdot \mathbf{n}) H] d\Gamma \quad (19)
\end{aligned}$$

It should be noted that the equation (16) is the same as the equation (16) in Wang, Zhou and Shan (2005). See Wang, Zhou and Shan (2005) for the explicit form of \mathbf{B}_J , $\bar{\mathbf{N}}$, \mathbf{D} , \mathbf{V}_I and \mathbf{V}_{dI} in 2D elasto-statics problem. Matrices $\bar{\mathbf{B}}_J$ and $\bar{\mathbf{V}}_{dI}$ are defined:

$$\bar{\mathbf{B}}_J = \begin{bmatrix} v_{1,1} \phi_{J,1} + v_{2,1} \phi_{J,2} & 0 \\ 0 & v_{1,2} \phi_{J,1} + v_{2,2} \phi_{J,2} \\ v_{1,2} \phi_{J,1} + v_{2,2} \phi_{J,2} & v_{1,1} \phi_{J,1} + v_{2,1} \phi_{J,2} \end{bmatrix} \quad (20)$$

$$\bar{\mathbf{V}}_{dI} = \begin{bmatrix} v_{1,1} N_{I,1} + v_{2,1} N_{I,2} & 0 \\ 0 & v_{1,2} N_{I,1} + v_{2,2} N_{I,2} \\ v_{1,2} N_{I,1} + v_{2,2} N_{I,2} & v_{1,1} N_{I,1} + v_{2,1} N_{I,2} \end{bmatrix} \quad (21)$$

For 2D cases, equation (16) denotes two algebraic equations containing $2N$ unknown nodal displacement sensitivities for one sub-domain. Loop over

all the sub-domains, the global algebraic system is obtained without ‘assembly’ process.

$$\mathbf{K}\dot{\mathbf{u}} = \mathbf{F}' \quad (22)$$

In above equation, matrix \mathbf{F}' is called external fictitious force [Bobaru and Mukherjee (2001)]. Matrix \mathbf{K} is the global stiffness matrix same as the stiffness matrix of structural analysis. Thus, the stiffness matrix in structural analysis stage can be stored and used for DSA purpose, which can reduce computational costs. By solving equation (22) for $\dot{\mathbf{u}}$, $\dot{\boldsymbol{\epsilon}}(u)$ and $\dot{\boldsymbol{\sigma}}(u)$ at any desired position can be approximated as:

$$\dot{\boldsymbol{\epsilon}}(u) = \sum_{I=1}^n \mathbf{B}_I \dot{\mathbf{u}}_I - \sum_{I=1}^n \bar{\mathbf{B}}_I \mathbf{u}_I \quad (23)$$

$$\dot{\boldsymbol{\sigma}}(u) = \mathbf{D}\dot{\boldsymbol{\epsilon}}(u) \quad (24)$$

From the equation (20)-(21), it is observed that the DSA results will strongly depend on the design velocity field. Applying an inappropriate velocity field may lead to inaccurate DSA results. Although the velocity field for a given problem is not uniquely defined, the design velocity field must meet both a regularity requirement and a linear dependency requirement [Ródenas, Fuenmayor and Tarancón (2004)]. For regularity requirement, the C^0 design velocity field with integrable first derivatives is required. The linear dependency requirement states that the design velocity fields must linearly depend on the variation of shape. There are several methods for computing the design velocity field. For example, boundary displacement method, isoparametric mapping method, Laplacian smoothing, exact differentiation of nodal co-ordinates and boundary mesh method are commonly used. Comparisons between these methods can be found in Ródenas, Fuenmayor and Tarancón (2004). The boundary displacement method [Chang, Choi, Tsai, Chen, Choi and Yu (1995); Ródenas, Fuenmayor and Tarancón (2004)] is used in this work. This method generates the velocity field by solving an auxiliary elasticity problem. As this method can simulate the natural deformation of the continuum structure, the obtained velocity field can be used to update the nodal position in optimization iterations.

The numerical implementation of DSA-LWF is quite easy, and can be summarized as several major steps shown in table 1.

4 Numerical results

Three numerical examples are presented to test the validity and accuracy of the proposed DSA-LWF approach. Three Gaussian points are used to evaluate domain integrals over each Delaunay triangle. For convergence study, the relative error of sensitivities [Fuenmayor, Oliver and Ródenas (1997); Ródenas, Fuenmayor and Tarancón (2004)] with respect to a given design variable α_m is defined:

$$\eta_m = \sqrt{\left| \frac{\chi_m^{\text{mathrme}} - \chi_m^n}{\chi_m^e} \right|} \quad (25)$$

where the superscripts e and n denote the exact solutions and numerical solutions, respectively. And χ_m is the sensitivity of the displacement norm:

$$\chi_m = \frac{\partial \|\mathbf{u}\|^2}{\partial \alpha_m} = \frac{\partial}{\partial \alpha_m} \left(\int_{\Omega} \mathbf{u}^T \mathbf{u} d\Omega \right) \quad (26)$$

As the non-Sibsonian interpolation only have C^0 continuity, a least square smoothing procedure is employed to recover nodal stresses and their sensitivities. The GiD [<http://gid.cimne.upc.es>] is used to visualize the results in the third numerical example.

4.1 The pulling of a bar

A bar with $E = 3 \times 10^7 \text{Pa}$ and $\nu = 0.3$ is subject to a uniaxial stress $t = 1.0 \times 10^4 \text{Pa}$ in the x direction at the free end. The dimensions of the bar and its boundary conditions are illustrated in figure 1(a). In this problem, the length of the bar l is chosen to be the design variable. A linear velocity distribution is used. The exact solution of displacement sensitivity is given in Bobaru and Mukherjee (2001). In the computation, irregular nodal arrangement with 68 nodes is used as shown in figure 1(b). The numerical solution for the displacement sensitivity \dot{u}_x along the x at the top edge are compared with the exact solution in figure 2.

Table 1: The pseudo code for DSA-LWF computation

Structural analysis, the stiffness matrix \mathbf{K} and nodal displacements are stored

Loop over all nodes

 Loop over all the included triangles and determine Gaussian points

 Loop over all the Gaussian points

 Loop over all the natural neighbours of the Gaussian point

 Compute the contribution to \mathbf{F}' (right hand of Eq.15)

 End loop over the natural neighbours

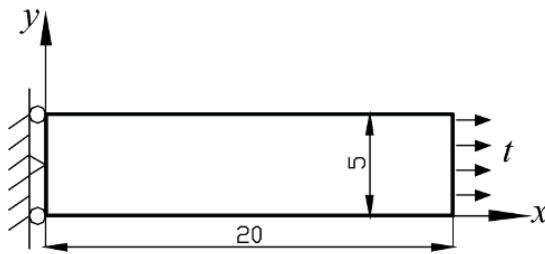
 End loop over Gaussian points

 End loop over triangles

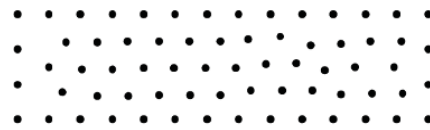
End loop over nodes

Solve the algebraic system (Eq.22) to get the nodal displacement sensitivities

Evaluate displacement or stress sensitivities at any given point



(a) Geometric model and its boundary conditions



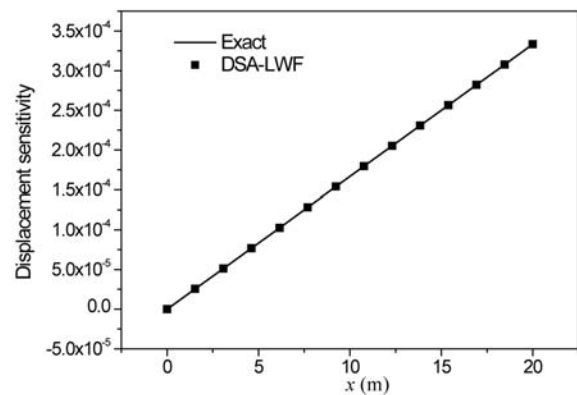
(b) The discrete model with 68 irregular nodes

Figure 1: The bar subject to a uniaxial stress

It can be seen that the DSA-LWF solution is in excellent agreement with the exact one.

4.2 *Lame's problem*

This problem is concerned with a thick cylinder of internal radius $a=1.0\text{m}$, and external radius $b=2.0\text{m}$, which is subjected to uniform internal pressure $p=1.0\text{Pa}$. Due to symmetry, only the upper right quadrant of the cylinder is modeled as shown in figure 3(a). Symmetrical conditions are imposed on the left and bottom edges. The internal radius a is chosen to be the design variable, and the geometry changes linearly with changes of the design variable a . The exact solution for displacement, stresses and their sensitivities are

Figure 2: Comparison of displacement sensitivity \dot{u}_x at the top edge of the bar

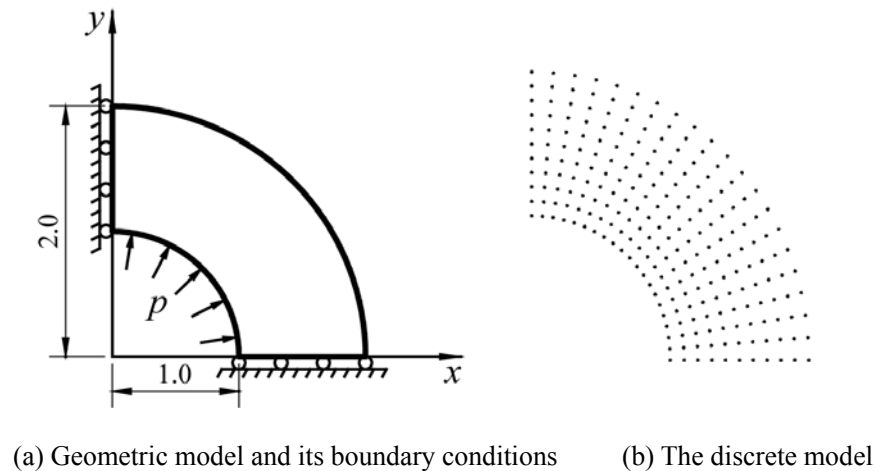


Figure 3: The Lamé's problem

given in Bobaru and Mukherjee (2001).

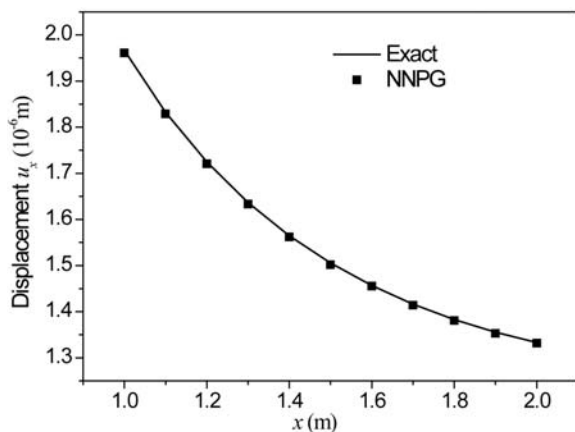


Figure 4: Displacement u_x along x -axis at $y=0.0$ m

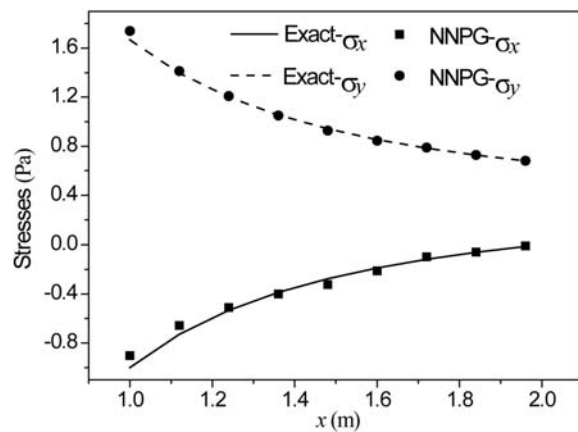


Figure 5: Stresses along x -axis at $y=0.0$ m

The plane strain condition is assumed with material properties $E = 1.0 \times 10^6$ Pa and $\nu=0.3$. In the computation, 11×21 regular nodal arrangement shown in figure 3(b) is used. The comparison between the exact and numerical results for displacement and stresses at $y=0.0$ m along x -axis are shown in figure 4-5. Excellent agreement between the numerical solutions and exact ones are achieved. The DSA-LWF displacement sensitivity at $y=0.0$ m along x -axis against exact one is shown in figure 6, from which we can see the two solutions almost match perfectly. In figure 7, the DSA-LWF stresses sensitivities at $y=0.0$ m along x -axis are compared with the exact ones. Obvi-

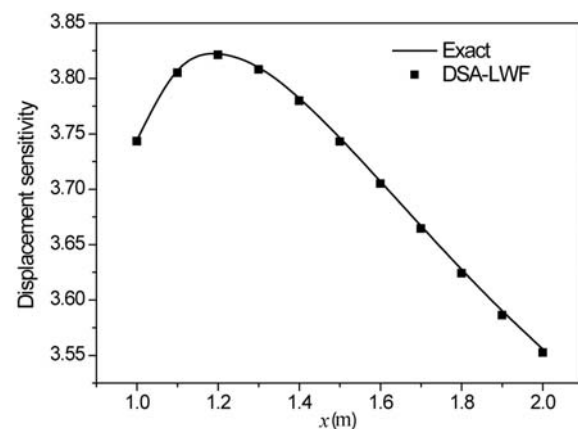


Figure 6: Displacement sensitivity \dot{u}_x along x -axis at $y=0.0$ m

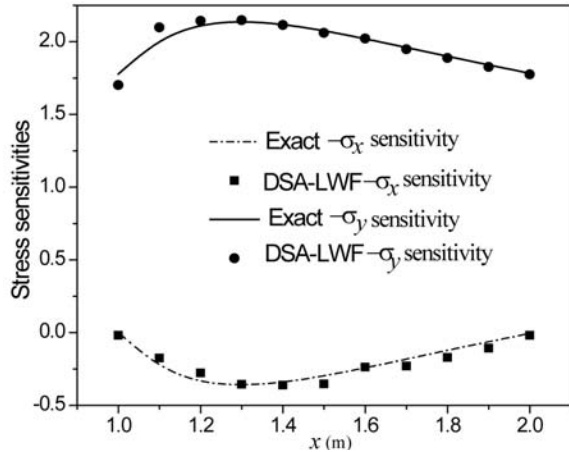


Figure 7: Stress sensitivities along x -axis at $y=0.0m$

ously, the accuracy of stress sensitivity is lower than that of displacement sensitivity.

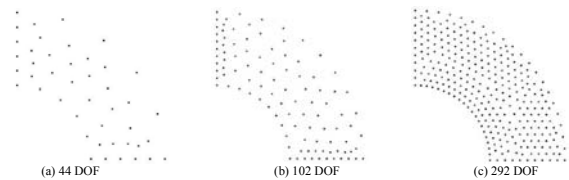


Figure 8: Nodal discretization for convergence study

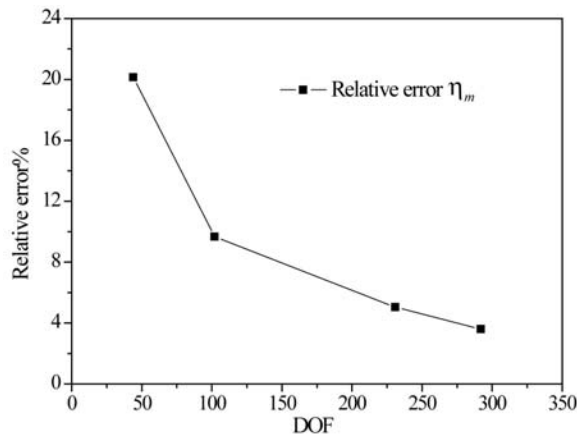


Figure 9: Evolution of η_m

Three irregular nodal arrangements shown in figure 8 and one regular nodal arrangement shown in

figure 3(b) are used to carry out the convergence study. Twenty-five Gaussian points are used to evaluate the relative errors. The evolution of the relative error in sensitivities η_m is illustrated in figure 9, from which we can observed that the relative error decreases when the DOF increases. The convergence rate slows down when the DOF exceeds 102, which may reflect the error introduced by the inexact numerical integration. This inexact numerical integration is mainly due to the non-polynomial form of the non-Sibsonian interpolation shape function [Cueto, Sukumar, Calvo, Ce-goñino and Doblaré (2003)].

4.3 Shape optimization of a fillet

The aim of this example is to find the optimal shape that minimizes the area without causing yielding anywhere in the bar. Here, the young's modulus, Poisson's ratio, admissible von Mises stress and traction are chosen to be $E = 1.0 \times 10^7 Pa$, $\nu = 0.3$, $[\sigma] = 120.0 Pa$ and $t = 100.0 Pa$, respectively.

Table 2: Coordinates of the control points

Control Nodes	Coordinates	Movable
A	(9.00, 9.00)	N
N_1	(10.30, 8.10)	Y
N_2	(12.25, 6.75)	Y
N_3	(14.20, 5.40)	Y
C	(15.50, 4.50)	N

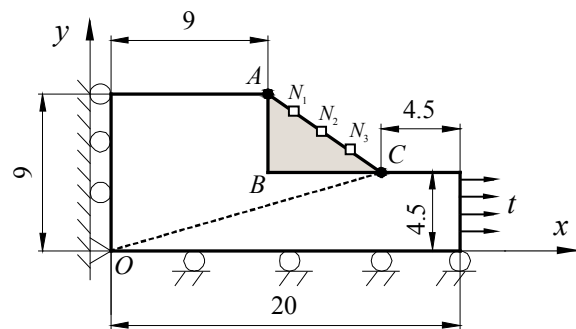


Figure 10: The geometric model, design boundary and boundary conditions

Due to symmetry, only the upper half of the structure is modeled as shown in figure 10. The seg-

ment AC is chosen to be the design boundary that can be varied during the optimization. Five control points are used to model the design boundary, namely A , N_1 , N_2 , N_3 and C . As shown in table 2, A and C are fixed, while N_1 , N_2 and N_3 are movable. The y -coordinates of movable points on the design boundary are chosen to be the design variables, i.e., $(y_{-N1}, y_{-N2}, y_{-N3})$. The initial values of design variables are $(8.10, 6.75, 5.40)$. With certain design parameterization method [Kim, Choi and Botkin (2003); Chang, Choi, Tsai, Chen, Choi and Yu (1995)], the design boundary can be expressed as the function of design variables, i.e. $p(y_{-N1}, y_{-N2}, y_{-N3})$. It is reported that the use of Akima spline interpolation as the design boundary representation can lead to the smooth design boundary after optimization [Bobaru and Mukherjee (2001)], and therefore the Akima spline interpolation is used in this work. As the minimization of the total area is equivalent to minimization of the area of triangle ΔABC , the objective function is chosen to be the area of triangle ΔABC . The inequality $g(y_{-N1}, y_{-N2}, y_{-N3})$ is that the maximum von Mises stress do not exceed the given admissible stress $[\sigma]$. The mathematical formulation of this optimization problem can be written as:

$$\min_{AC} A_{\Delta ABC} = \int p(y_{-N1}, y_{-N2}, y_{-N3}) dx - 4.5 \times 6.5 \quad (27a)$$

$$s.t. g(y_{-N1}, y_{-N2}, y_{-N3}) = 1 - \frac{\sigma_{max}}{[\sigma]} \geq 0 \quad (27b)$$

$$4.5 \leq y_{-Ni} \leq 9.0, \quad i = 1, 2, 3 \quad (27c)$$

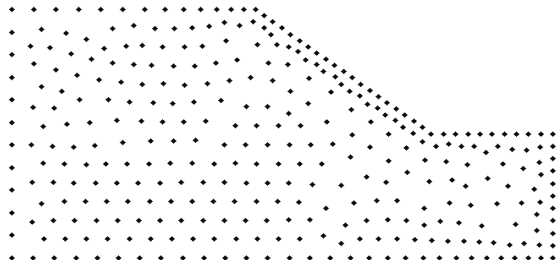


Figure 11: The discrete model with 339 irregular nodes

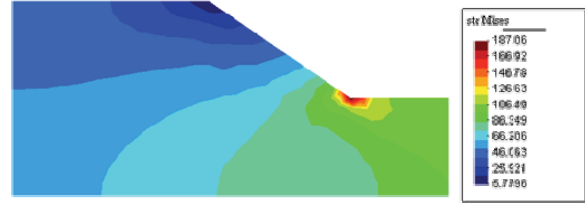
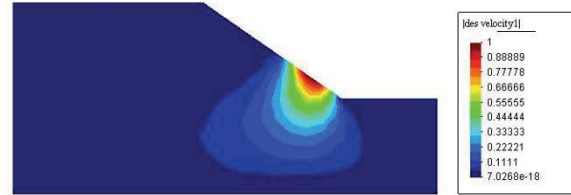
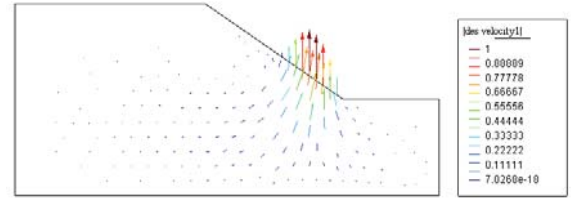


Figure 12: The distribution of von Mises stress of initial design



(a) Contour plot



(b) Vector plot

Figure 13: The velocity field v_{sum} computed using boundary displacement method

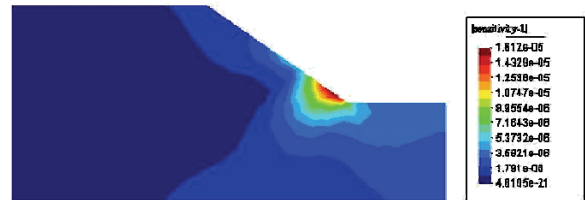


Figure 14: The displacement sensitivity u_{sum} obtained using DSA-LWF

The structure analysis is solved for plane strain case. The nodal arrangement is shown in figure 11, which have 339 irregular nodes. There are 21 nodes are equal-space placed on the design boundary. Among these nodes, the 1st, 5th, 11th, 17th and 21st nodes are corresponding to the control points A , N_1 , N_2 , N_3 and C respectively. The stress distribution of the initial structure is shown in figure 12. The severe stress concentration is observed and the maximum stress is 187.06Pa,

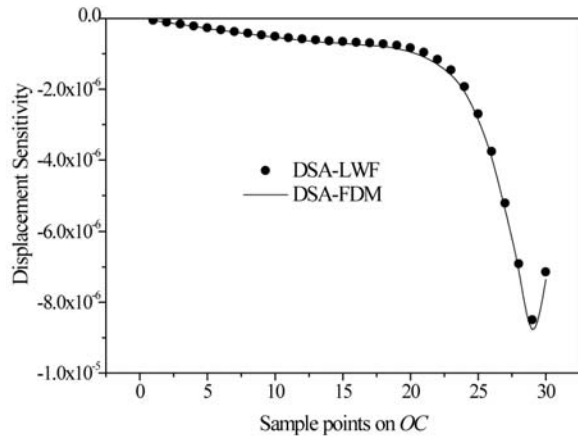


Figure 15: Displacement sensitivity \dot{u}_x along the line OC

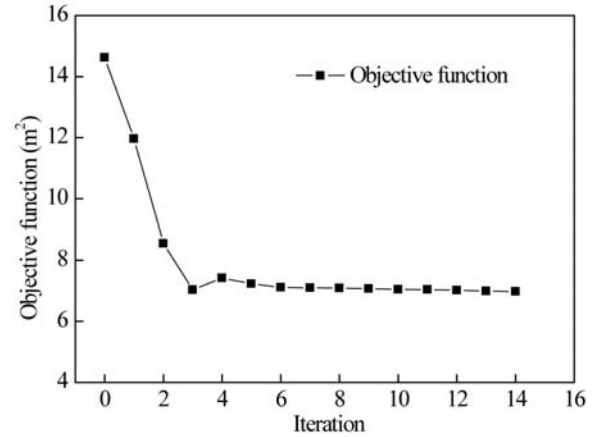


Figure 17: The iteration history

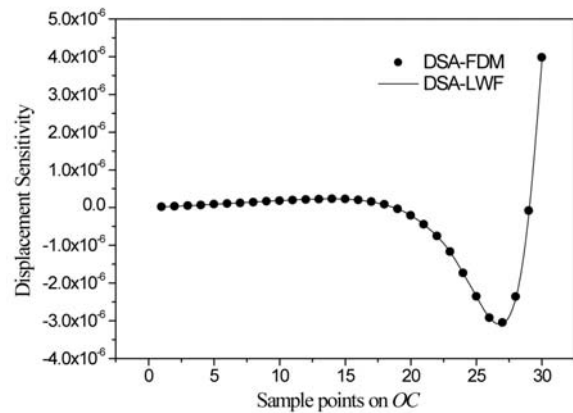


Figure 16: Displacement sensitivity \dot{u}_y along the line OC

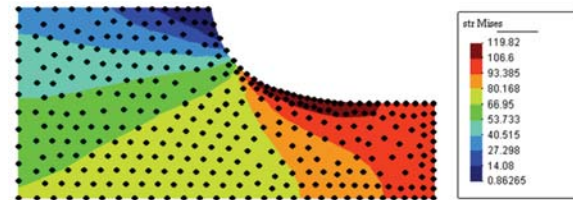


Figure 18: The final optimal design: The geometric model, discrete model and the distribution of von-Mises stress of the optimal design

which exceeds the admissible one by over fifty percent. The design velocity field (vector sum) with respect to design variable y_{N3} of the initial design is shown in figure 13. As we can see, the velocity value at the control point N_3 is unity and decreases to zero as the distance from that control point increases. The distribution of displacement sensitivity (vector sum) with respect to design variable y_{N3} is illustrated in figure 14. The displacement sensitivity component \dot{u}_x and \dot{u}_y along the line OC obtained by the DSA-LWF are compared with those obtained by the finite difference method (FDM, perturbation=0.001) in figure 15-16, where perfect matches are observed.

Due to the nonlinear property of shape optimization problem, the Sequential Quadratic Program-

ming method (SQP) in Bobaru and Mukherjee (2001) is used to solve the minimization problem. In figure 17, the iteration history for the objective function is illustrated. From this figure, we can observe that the value of objective function is decrease from $14.625m^2$ to $7.03m^2$ after only four iterations, which is quite close to the optimal value, i.e., $6.98m^2$. The high convergence rate benefits from the accurate sensitivities obtained from DSA-LWF. In figure 18, the optimal design is illustrated, where no oscillating design boundary is observed. The severe stress concentration disappeared and there are 13 nodes out of 21 nodes on the design boundary whose von Mises stresses approach admissible one. Satisfied result is obtained after the optimization even though only three design variables are used. Also, the optimization process is totally automatic, and absolutely no remeshing processes are needed.

5 Conclusions

The design sensitivity analysis method based on the local weak form (DSA-LWF) is proposed in this paper. The numerical examples show the obtained DSA-LWF solutions are valid and accurate. This method possesses the following properties:

- (1) No additional background meshes are needed to integrate the weak form and no assembly process is needed to generate the global stiffness matrix because the local weak form is used instead of global weak form. No user-defined parameters (e.g., penalty parameter and size of supports of weight functions) are needed.
- (2) More accurate solution can be obtained, as the differentiation is taken before the discretization. The calculation of derivatives of shape functions with respect to design variables is avoided.
- (3) Drawbacks related to the use of FEM are eliminated because the NNPG is used to discretize the continuous form of DSA formulation. The accuracy of the DSA-LWF solutions will not degenerate during optimization iteration as no explicit mesh is needed to interpolate the field variable and their sensitivities.
- (4) The numerical implementation of this method is quite easy and can be integrated into the NNPG code, where the stiffness matrix of the structural analysis can be stored and reused in DSA calculation.

Acknowledgement: The authors would like to acknowledge the support of the National Science Foundation of China (10572077), the Chinese Ministry of Education University Doctoral Research Foundation (20060422013), and the Natural Science Foundation of Shandong Province (Y2007F20).

References

Andreas, U.; Batra, R. C.; Porfiri, M. (2005): Vibrations of cracked Euler-Bernoulli beams us-

ing Meshless Local Petrov-Galerkin (MLPG) method, *CMES: Computer Modeling In Engineering & Sciences*, vol. 9 no. 3, pp. 111-131.

Atluri, S. N.; Zhu, T. (1998): A new meshless local Petrov-Galerkin (MLPG) approach in computational mechanics, *Computational Mechanics*, vol. 22, pp. 117-127.

Atluri, S. N.; Kim, H. G.; Cho, J. Y. (1999): A critical assessment of the truly meshless local Petrov-Galerkin (MLPG) and local boundary integral equation methods, *Computational Mechanics*, vol. 24, pp. 348-372.

Atluri, S. N.; Shen, S. (2002): The meshless local Petrov-Galerkin (MLPG) method: a simple and less-costly alternative to the finite element and boundary element methods, *CMES: Computer Modeling in Engineering & Sciences*, vol. 3 no.1, pp. 11-51.

Atluri, S. N.; Han, Z. D.; Rajendran, A. M. (2004): A new implementation of the meshless finite volume method, through the MLPG "Mixed" approach, *CMES: Computer Modeling in Engineering & Sciences*, vol. 6 no. 6, pp. 491-513.

Atluri, S. N.; Liu, H. T.; Han, Z. D. (2006a): Meshless local Petrov-Galerkin (MLPG) mixed collocation method for elasticity problems, *CMES: Computer Modeling in Engineering & Sciences*, vol. 14 no. 3, pp. 141-152.

Atluri, S. N.; Liu, H. T.; Han, Z. D. (2006b): Meshless local Petrov-Galerkin (MLPG) mixed finite difference method for solid mechanics, *CMES: Computer Modeling in Engineering & Sciences*, vol. 15 no. 1, pp. 1-16.

Belytschko, T.; Lu, Y.; Gu, L. (1994): Element free Galerkin methods, *International Journal for Numerical Methods in Engineering*, vol. 37 no. 2, pp. 229-256.

Belytschko, T., Krongauz, Y., Organ, D., Fleming, M., Krysl, P. (1996): Meshless methods: An overview and recent developments, *Computer Methods in Applied Mechanics and Engineering*, vol. 139, pp. 3-47.

Bobaru, F.; Mukherjee, S. (2001): Shape sensitivity analysis and shape optimization in planar elasticity using the element-free Galerkin method, *Computer Methods in Applied Mechanics and En-*

gineering, vol. 190, pp. 4319-4337.

Bobaru, F.; Mukherjee, S. (2002): Meshless approach to shape optimization of linear thermoelastic solid, *International Journal for Numerical Methods in Engineering*, vol. 53 no. 4, pp. 765-796.

Chang, K. H.; Choi, K. K.; Tsai, C. S.; Chen, C. J.; Choi, B. S.; Yu, X. (1995): Design sensitivity analysis and optimization tool (DSO) for shape design applications, *Computing Systems in Engineering: An International Journal*, vol. 6 no. 26, pp. 151-175.

Ching, H. K.; Chen, J. K. (2006): Thermomechanical analysis of functionally graded composites under laser heating by the MLPG method, *CMES: Computer Modeling In Engineering & Sciences*, vol. 13 no. 3, pp. 199-217.

Cueto, E.; Sukumar, N.; Calvo, B.; Cegoñino, J.; Doblaré, M. (2003): Overview and Recent Advances in Natural Neighbour Galerkin Methods, *Archives of Computational Methods in Engineering*, vol. 10 no. 4, pp. 307-384.

Dolbow, J.; Belytschko, T. (1999): Numerical Integration of the Galerkin Weak Form in Mesh-free Methods, *Computational Mechanics*, vol. 23, pp. 219-230.

Fuenmayor, F. J.; Oliver, J. L.; Ródenas, J. J. (1997): Extension of the zienkiewicz-zhu error estimator to shape sensitivity analysis, *International Journal for Numerical Methods in Engineering*, vol. 40 no. 8, pp. 1413-1433.

Gao, L.; Liu, K.; Liu, Y. (2006): Applications of MLPG method in dynamic fracture problems, *CMES: Computer Modeling in Engineering & Sciences*, vol. 12 no. 3, pp. 181-195.

GiD: The personal pre and postprocessor. <http://gid.cimne.upc.es>

Grindeanu, I.; Kim, N. H.; Choi, K. K.; Chen, J. S. (2002): CAD-based shape optimization using a meshfree method, *Concurrent Engineering Research and Applications*, vol. 10 no. 1, pp. 55-66.

Han, Z. D.; Atluri, S. N. (2004): Meshless local Petrov-Galerkin (MLPG) approaches for solving 3D problems in elasto-statics, *CMES: Computer*

Modeling in Engineering & Sciences, vol. 6 no.2, pp. 169 -188.

Han, Z. D.; Rajendran, A. M.; Atluri, S. N. (2005): Meshless Local Petrov-Galerkin (MLPG) approaches for solving nonlinear problems with large deformations and rotations, *CMES: Computer Modeling in Engineering & Sciences*, vol. 10 no. 1, pp. 1-12.

Han, Z. D.; Liu, H. T.; Rajendran, A. M.; Atluri, S. N. (2006): The applications of meshless local Petrov-Galerkin (MLPG) approaches in high-speed impact, penetration and perforation problems. *CMES: Computer Modeling in Engineering & Sciences*, vol. 14 no. 2, pp. 119-128.

Jarak, T.; Soric, J.; Hoster, J. (2007): Analysis of shell deformation responses by the meshless local Petrov-Galerkin (MLPG) approach, *CMES: Computer Modeling in Engineering & Sciences*, vol. 18 no. 3, pp. 235-246.

Kim, N. H.; Yi, K.; Choi, K. K. (2002): A material derivative approach in design sensitivity analysis of three-dimensional contact problems, *International Journal of Solids and Structures*, vol. 39 no. 8, pp. 2087-2108.

Kim, N. H.; Choi, K. K.; Botkin, M. E. (2003): Numerical method for shape optimization using meshfree method, *Structural and Multidisciplinary Optimization*, vol. 24 no. 6, pp. 418-429.

Lacroix, D.; Bouillard, P. (2003): Improved sensitivity analysis by a coupled FE-EFG method, *Computers and Structures*, vol. 81 no. 26-27, pp. 2431-2439.

Liu, W. K.; Jun, S.; Zhang, Y. F. (1995): Reproducing kernel particle methods, *International Journal for Numerical Methods in Fluids*, vol. 20 no. 8-9, pp. 1081-1106.

Ródenas, J. J.; Fuenmayor, F. J.; Tarancón, J. E. (2004): A numerical methodology to assess the quality of the design velocity field computation methods in shape sensitivity analysis, *International Journal for Numerical Methods in Engineering*, vol. 59 no.13, pp. 1725-1747.

Shen, S. P.; Atluri, S. N. (2004): Multiscale simulation based on the meshless local Petrov-Galerkin (MLPG) method, *CMES: Computer Modeling in Engineering & Sciences*, vol. 5 no.

3, pp. 235-255.

Sladek, J.; Sladek, V.; Zhang C, Solek, P. (2007): Application of the MLPG to thermo-piezoelectricity, *CMES: Computer Modeling in Engineering & Sciences*, vol. 22 no. 3, pp. 217-233.

Timoshenko, S.P.; Goodier, J.N. (1970): *Theory of Elasticity*, 3rd edition, McGraw Hill.

Vavourakis, V.; Sellountos, E. J.; Polyzos, D. (2006): A comparison study on different MLPG(LBIE) formulations, *CMES: Computer Modeling in Engineering & Sciences*, vol. 13 no. 3, pp. 171-183.

Vavourakis, V.; Polyzos, D. (2007): A MLPG4 (LBIE) formulation in elastostatics, *CMC: Computers Materials & Continua*, vol. 5 no. 3, pp. 185-196.

Wang, K.; Zhou, S. J.; Shan, G. J. (2005): The natural neighbour Petrov-Galerkin method for elasto-statics, *International Journal for Numerical Methods in Engineering*, vol. 63 no. 8, pp. 1126-1145.

